

Determination of antiferromagnetic coupling constants in the spin-dimer compound β - $\text{Sr}_2\text{Cu}(\text{BO}_3)_2$

N. McCrate^a and S. Hill^b

^a Science Division, Truman State University, Kirksville, MO 63501

^b Department of Physics, University of Florida, Gainesville, FL 32611

Abstract

Electron Spin Resonance was used to study the spin-dimer compound β - $\text{Sr}_2\text{Cu}(\text{BO}_3)_2$.

The value of the antiferromagnetic coupling constant (J) between the copper dimers was estimated from temperature-dependence measurements to be 92 K at a frequency of 111.3 GHz and 91 K at a frequency of 66.7 GHz.

Introduction

From refrigerator magnets to hard drives, magnetism is a familiar phenomenon. The source of the unique behavior of everyday magnetic materials is the spontaneous, parallel alignment of unpaired electron spins on neighboring atoms. This type of magnetism is called ferromagnetism. An equally common yet very different form of magnetism is antiferromagnetism. Like ferromagnetism, antiferromagnetism arises due to the spontaneous alignment of unpaired electron spins on neighboring atoms, but the alignment of spins in antiferromagnetic materials is anti-parallel.

In both ferromagnetic and antiferromagnetic (AF) spin systems, exchange interactions cause spontaneous spin alignment. A purely quantum-mechanical phenomenon, exchange occurs when the wavefunctions of two or more fermions, particles having half-integer spins, overlap; this results in a change in the fermions' energies. The term describing exchange

interactions in an effective Hamiltonian for pairs of electrons in a many-electron system is of the form

$$\hat{H} = -2 \sum_{i>j} J_{ij} \mathbf{S}_i \cdot \mathbf{S}_j \quad (1)$$

where J_{ij} is the exchange constant between the i^{th} and j^{th} spins, \mathbf{S}_i is the spin operator for the i^{th} spin, and \mathbf{S}_j is the spin operator for the j^{th} spin. The sign of J indicates whether a system is ferromagnetic, $J > 0$, or AF, $J < 0$.

AF spin systems exhibit additional order depending on the magnitude of the exchange constant between adjacent spins (J, J', J'' , etc.) (Figure 1). If J, J' and J'' are approximately equal, then the spin system exhibits Néel order. In Néel ordered systems, the exchange interactions cause the spins to align antiparallel. If J is much larger than J' or J'' , then the spins still align antiparallel, but J dominates, and we consider the two ions to behave as one entity, called a singlet pair or spin dimer.

To better understand spin dimers, let us consider a two-spin AF system. Two possible degenerate states exist in the absence of mixing: $|\uparrow\downarrow\rangle$ and $|\downarrow\uparrow\rangle$ where \uparrow symbolizes a spin-up electron with $m_s = +1/2$, and \downarrow symbolizes a spin-down electron with $m_s = -1/2$. When quantum-mechanical mixing of states occurs, a ground state of $|\uparrow\downarrow\rangle - |\downarrow\uparrow\rangle$ results. The mixed ground state is described spectroscopically as a singlet pair and may be visualized as two $S=1/2$ spins combining to form an $S=0$ bosonic spin dimer. Because spin-dimer formation involves a single, strong interaction between only two $S=1/2$ spins, interactions with neighboring spins often preclude spin-dimer formation in macroscopic systems.

Spin-dimer compounds sometimes exhibit a large energy separation between their ground and triplet states. Because this energy separation is associated with the spin degrees of freedom, it is called a spin gap. To the first order the size of the spin gap depends on J ; however, as J' and

J'' increase the spin gap decreases. Thus, spin gaps are believed to be related to the extent of dimer localization; the greater the dimer localization the greater the spin gap.

β - $\text{Sr}_2\text{Cu}(\text{BO}_3)_2$, an inorganic spin-gap compound, was studied to better understand the spin-dimer phenomenon. The β - $\text{Sr}_2\text{Cu}(\text{BO}_3)_2$ crystal lattice is comprised of alternating layers of $\text{Cu}_2\text{B}_4\text{O}_{12}$ units separated by Sr^{2+} ions [1]. Within the crystal lattice, there are both octahedral and square planar copper coordination sites (Figure 2) [1]. Copper dimers are formed through an octahedrally coordinated copper exchange coupling to a square planarly coordinated copper through its equatorial oxygen atoms [2]. Although this exchange coupling is the strongest, there are two other inter-dimer exchange pathways, J' and J'' [2]. At high temperatures and low magnetic fields, the effects of J' and J'' are negligible; however, under conditions of low temperatures and high magnetic fields, J' and J'' play a more significant role in the behavior of β - $\text{Sr}_2\text{Cu}(\text{BO}_3)_2$, as illustrated by a reduction in the spin gap.

Electron Spin Resonance Spectroscopy

Electron Spin Resonance (ESR) spectroscopy observes the photon-induced excitations of unpaired electron spins. In a typical ESR experiment, absorption spectra are collected by placing a sample in a magnetic field and sweeping the magnetic field while irradiating the sample with constant-frequency microwave radiation. From the data, a phenomenological equation called a spin Hamiltonian is developed to describe the observed spectra. The spin Hamiltonian always contains a Zeeman term of the form

$$\hat{H} = \vec{g}\mu_B B \hat{S}_z \quad (2)$$

where \vec{g} is the g-tensor describing the angle dependence of the peak position, μ_B is the Bohr magneton, B is the magnetic field, and \hat{S}_z is the z component of the spin angular momentum

operator. Other terms may be added to the spin Hamiltonian as needed to fully describe the observed spectra.

Once a spin Hamiltonian has been developed, determination of J , J' , and J'' is possible using the VanVleck equation in conjunction with the spin Hamiltonian. The VanVleck equation quantitatively describes the temperature-dependent paramagnetic susceptibility of magnetic materials if the energy levels of the spin transitions are known. Because, at low fields, EPR signal intensities are proportional to the paramagnetic susceptibility of the material and the energy levels of the transitions are given by the spin Hamiltonian, it is possible to determine J , J' , and J'' by measuring the temperature dependence of the EPR signal intensity.

Experimental Equipment and Procedures

We employed the cavity perturbation method described in Mola *et al.* for EPR spectra collection [3]. In an axial cylindrical resonant cavity, we placed a single crystal of β - $\text{Sr}_2\text{Cu}(\text{BO}_3)_2$ on a quartz pillar attached to the base plate (Figure 3). A millimeter vector network analyzer (MVNA) both generated and detected microwave signal. Rectangular waveguides transmitted the microwave signal to the cavity.

A Quantum Design Physical Property Measurement System (PPMS) with a superconducting 7 T split-solenoid magnet supplied the magnetic field. For angle-dependence measurements, we changed the probe angle using a rotating cuff controlled through the PPMS. The sample space of the PPMS is thermally isolated from the magnet. We controlled sample-space temperature through the PPMS using a combination of heaters and cold helium gas flow.

We performed angle-dependence measurements at 2.5 K, 5 K, and 25 K using a microwave frequency of 51.217 GHz. For each measurement, we collected spectra at 10° increments over a 180° rotation. In the 2.5-K, 5-K, and 25-K experiments, we swept the magnetic field from 1.5 T to 1.9 T, 1.0 T to 2.5 T, and 1.3 T to 2.0 T respectively.

We measured the temperature dependence of spectra peak intensities along the hard axis at 66.7 GHz and 111.3 GHz. The easy and hard axes describe the directions in which the spin excitations are observed at the lowest and highest magnetic fields respectively. For the 66.7-GHz measurements, we swept the magnetic field from 2.25 T to 2.55 T over a temperature range of 2.5 K to 234 K. In the 111.3-GHz measurements we swept the magnetic field from 3.50 T to 4.20 T over a temperature range of 5 K to 150 K. We collected spectra at two different frequencies because saturation was suspected at 66.7 GHz due to strong energy absorption. There are two types of saturation possible in this experiment: saturation caused by the excitation of too many molecules resulting in decreased probability of transition to the excited state and saturation caused by the sample creating a signal outside of the optimum detection range of the MVNA. Due to the large size of the crystal used, it is likely that saturation was due to the latter.

Angle-Dependence Results

The ESR spectra of β - $\text{Sr}_2\text{Cu}(\text{BO}_3)_2$ exhibit two distinct peak types (Figure 4). Below approximately 10 K the spectra are dominated by hyperfine-splitting peaks. The hyperfine-splitting peaks are not caused by the spin dimers because spin dimers do not exhibit hyperfine splitting. Thus, the hyperfine-splitting peaks are due to the presence of spin- $1/2$ impurities. Above 17 K, the spectra are dominated by a single large peak attributable to triplet excitations of copper spin dimers (Figure 5).

We used the angle-dependence measurements at 25 K to establish the directions of the easy and hard axes of the sample. To find the peak positions as a function of field for rotation in a single plane, we combine two equations: the energy due to Zeeman splitting of electron spins, $\Delta E = g(\theta)\mu_b B$ where ΔE is the transition energy between levels and $g(\theta)$ is the angle dependence of the peak position given by $g(\theta) = \langle g \rangle + \delta g \cos \theta$ where $\langle g \rangle$ is the average g -value; and the energy of a photon $E = h\nu$, giving

$$B(\theta) = \frac{h\nu}{\mu_b(\langle g \rangle + \delta g \cos \theta)}. \quad (3)$$

Equation (3) may be rearranged to give a fitting function of the form

$$B(\theta) = \frac{A}{1 + B \cos(\theta)}. \quad (4)$$

By plotting peak position as a function of angle, and fitting Equation (4) to the data, we find the angle of maximum and minimum field peak positions by taking the first derivative of the resulting function (Figure 6). We used the positions of the easy and hard axes to orient the sample in the temperature-dependence experiments.

The angle-dependence spectra collected at 2.5 K exhibit two sets of four peaks (Figure 7). These two sets of four peaks come together and split apart during the 180° rotation of the sample. It is well established in the literature that hyperfine splitting due to individual copper (II) ions creates four EPR-observable peaks. The presence of two distinct sets of four peaks suggests that the hyperfine splitting may be due to broken copper dimers in two different orientations.

Additional peaks in the wings of the 2.5 K spectra prompted another angle-dependence study over a broader field range at 5 K. We observed two different sets of maxima and minima in the peaks of the angle-dependence data, as illustrated by the colored lines in Figure 8. These sets of peaks likely correspond to two spin-one impurities in two different orientations; however,

the identity of the impurity is unknown. It is possible that the spin-one impurity is attributable to ferromagnetic coupling between a limited number of copper ions.

Temperature-Dependence Results

To check for saturation in the temperature-dependence data, we plotted signal intensity as a function of temperature for the spectra collected at 66.7 GHz and 111.3 GHz. The intensities collected at 111.3 GHz were scaled at low temperature to match those collected at 66.7 GHz. Saturation occurred at 66.7 GHz as illustrated by the 111.3-GHz spectra exhibiting a much larger maximum intensity than that of the 66.7 GHz spectra (Figure 9).

Accurate determination of J , J' , and J'' requires a spin Hamiltonian containing parameters for J , J' , and J'' ; however, we have not determined terms for J' and J'' in the β - $\text{Sr}_2\text{Cu}(\text{BO}_3)_2$ system. Assuming J' and J'' are negligible, we may roughly approximate J using a previously developed fitting function based on the VanVleck equation in conjunction with a spin Hamiltonian containing only Zeeman and exchange terms. By accounting for contribution of spin-half impurities to the signal intensity, this fitting function allows the estimation of spin-half impurity concentrations. The following fitting function was used to fit both the 66.7-GHz and 111.3-GHz data:

$$I = C \left(\sqrt{2}(1 - \alpha) \frac{e^{1/x} - e^{-1/x}}{1 + e^{J/(g\mu_B Bx)} + e^{1/x} + e^{-1/x}} + \alpha \frac{e^{0.5/x} - e^{-0.5/x}}{e^{0.5/x} + e^{-0.5/x}} \right) \quad (5)$$

where I is the signal intensity, C is a parameter, α is the fraction of spin-half impurities, and $x = k_B T (g\mu_B B)^{-1}$ (Figure 10). Although some saturation occurred in the 66.7-GHz spectra, these data were still used to calculate a J value because they produced good signals at low and high

temperatures. At 66.7 GHz, we found $J = 91$ K and $\alpha = 0.33\%$, and at 111.3 GHz, we found $J = 92$ K and $\alpha = 0.26\%$.

Future Plans

Due to time constraints, the β - $\text{Sr}_2\text{Cu}(\text{BO}_3)_2$ crystal we studied had not been characterized by X-ray crystallography. Crystallographic data allow for absolute orientation of the sample, possibly identify lattice defects and impurities, and ensure that the crystal studied is of good quality. Future studies will measure the properties of the system relative to the crystallographic axes.

Although we conjectured about the source of the small peaks observed at 5 K, the true source of these peaks remains unknown. Because only one crystal was measured, we are not sure if these peaks come from unique defects in the studied sample crystal or are common to all β - $\text{Sr}_2\text{Cu}(\text{BO}_3)_2$ crystals. Measurement of additional β - $\text{Sr}_2\text{Cu}(\text{BO}_3)_2$ crystals will answer this question. If these peaks are indeed due to the β - $\text{Sr}_2\text{Cu}(\text{BO}_3)_2$ lattice, then frequency-dependence measurements will be necessary to determine which energy transitions these peaks are attributable to.

Figure 10 (b) shows that Equation (5) fits poorly the temperature-dependence data near the maximum signal intensity. The poor fit of Equation (5) indicates our assumption about the negligibility of J' and J'' was incorrect and confirms that the effects of J' and J'' are significant under low-temperature, high-field conditions. To improve the fit and accurately measure the values of J , J' , and J'' , we must develop a spin Hamiltonian that includes terms for J' and J'' .

Acknowledgments

We would like to thank to Sung Su Kim for useful discussions and Changhyun Koo for help with the EPR instrumentation. This work was supported by an NSF REU grant at the University of Florida.

References

- [1] W. Smith and D. A. Keszler, *J. Solid State Chem.* **81**, 305 (1989).
- [2] S.E. Sebastian, D. Yin, P. Tanedo, N. Harrison, G. Jorge, M. Jaime, Y. Mozzerov, G. Miller, and I. R. Fisher, *Phys. Rev. B.* **71**, 212405 (2005).
- [3] M. Mola, S. Hill, P. Goy, and M. Gross, *Rev. Sci. Inst.* **71**, 186 (2000).

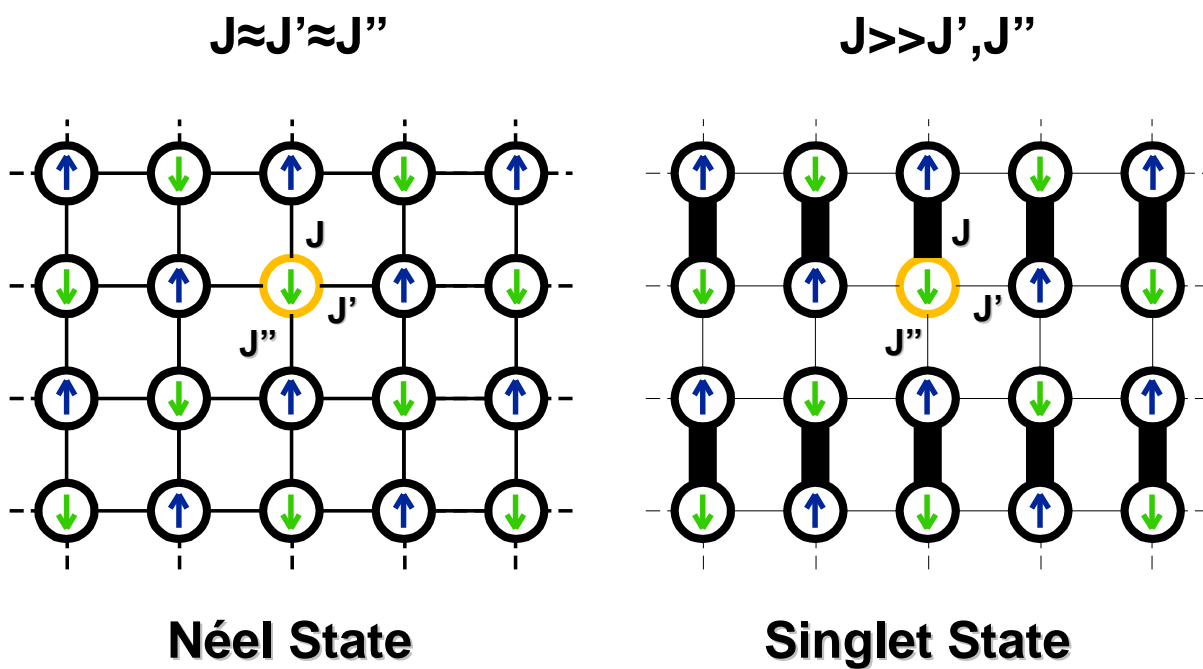


Fig. 1. Two types of order possible for antiferromagnets.

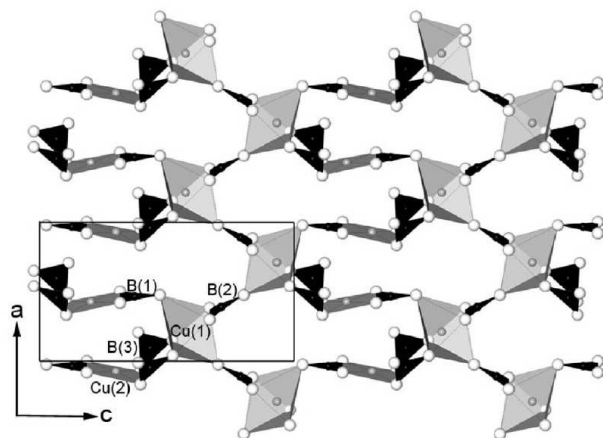
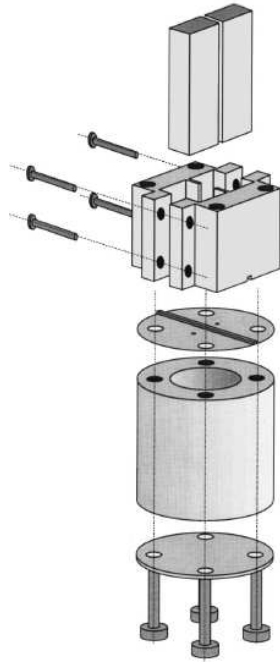


Fig. 2. Sr₂Cu(BO₃)₂ crystal lattice. (Figure reproduced from Sebastian *et al.*, 2005.)

a)



b)

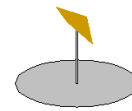


Fig. 3. a) Schematic of cylindrical resonant cavity. (Figure reproduced from Mola *et al.*, 2000.)
b) Schematic of sample mounted on quartz pillar in base plate of resonant cavity.

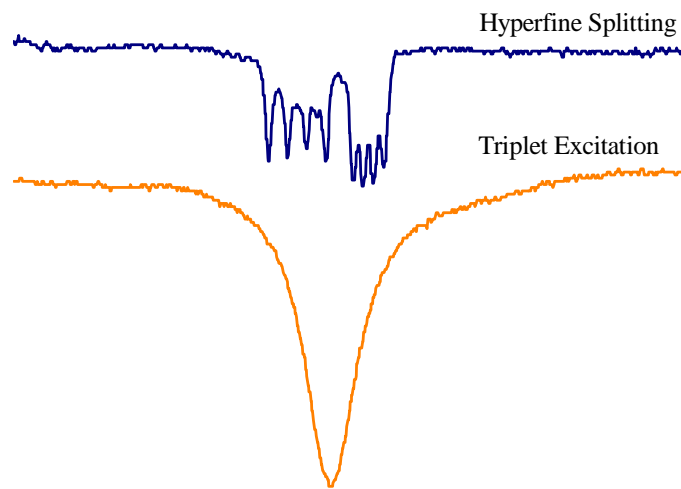


Fig. 4. Examples of hyperfine-splitting peaks and triplet-excitation peaks.

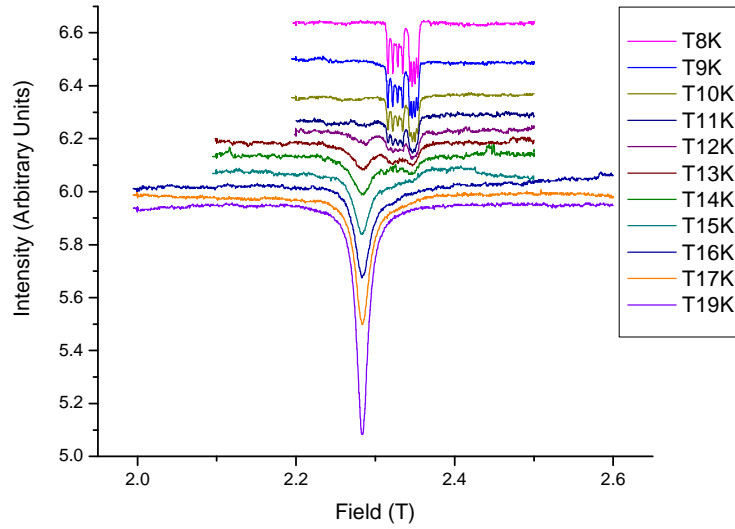


Fig. 5. Temperature-dependence spectra showing the shift from hyperfine-splitting peaks to a single triplet-excitation peak.

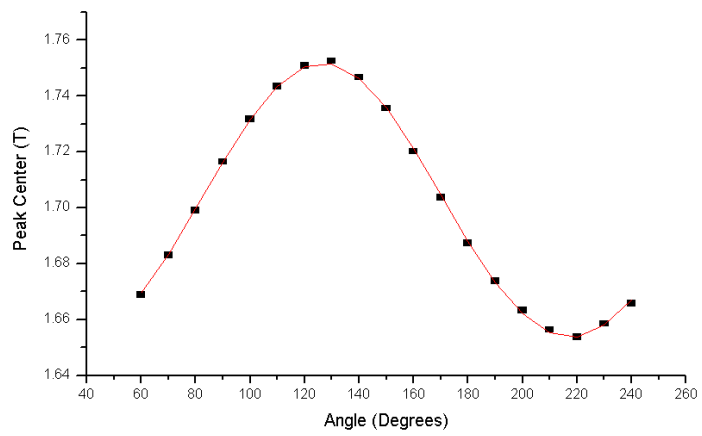


Fig. 6. Angle dependence of the triplet-excitation peak at 25 K fitted to Eq. (4).

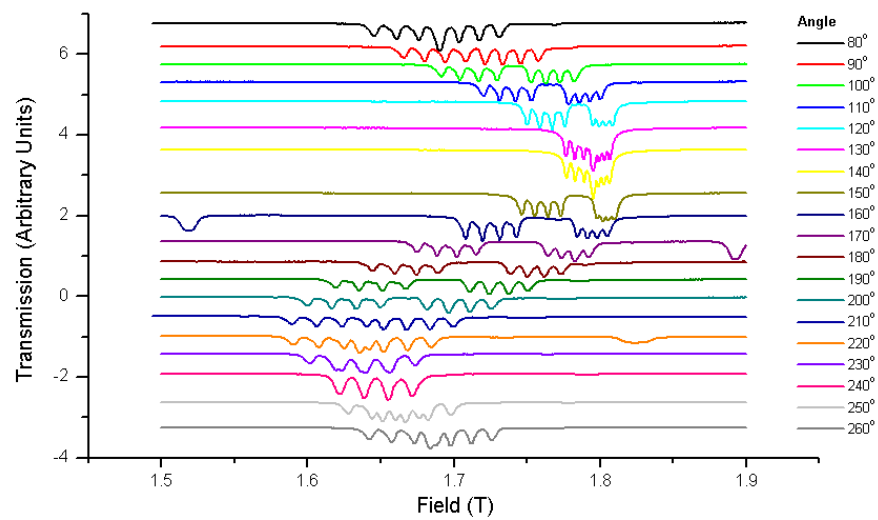


Fig. 7. Angle dependence of hyperfine peak spectra at 2.5 K

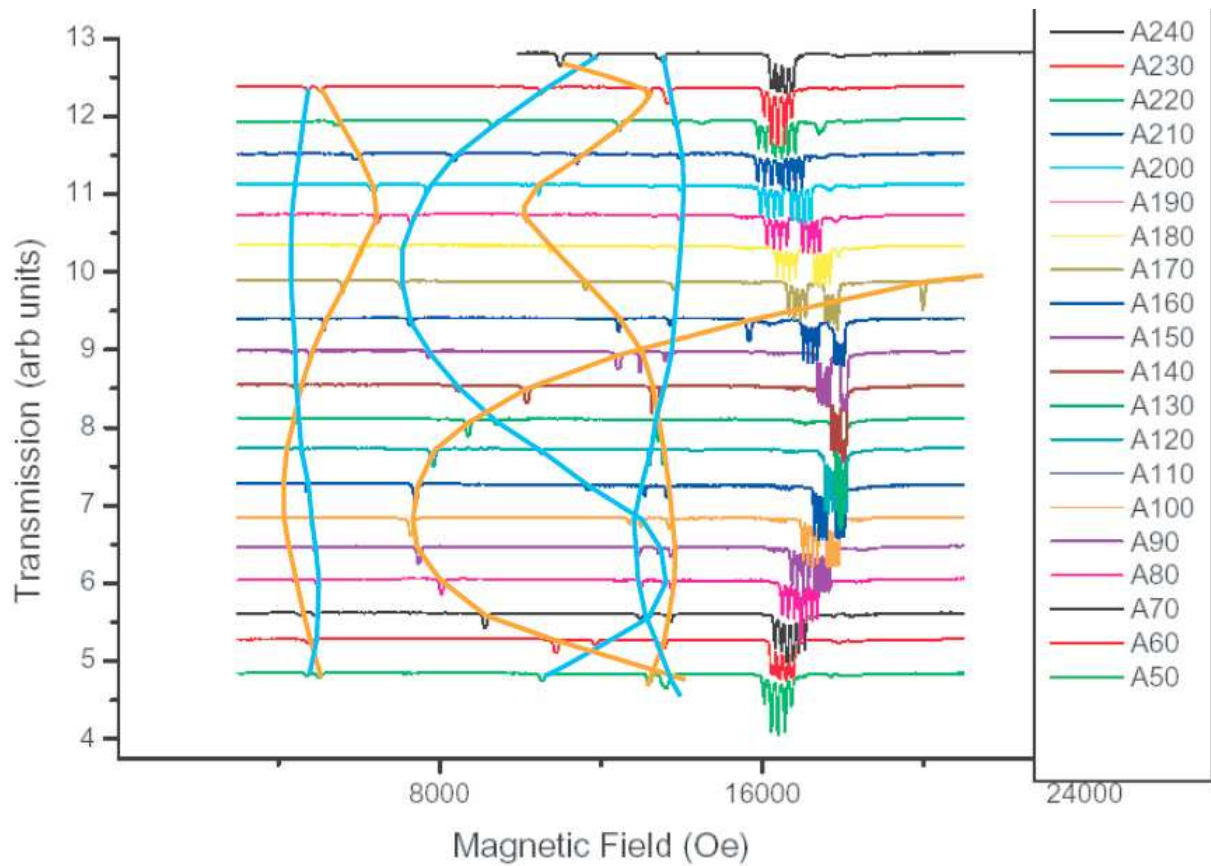


Fig. 8. Angle dependence of additional peaks 5 K. Blue and orange lines illustrate the two different sets of maxima and minima observed in the angle dependence of the peaks.

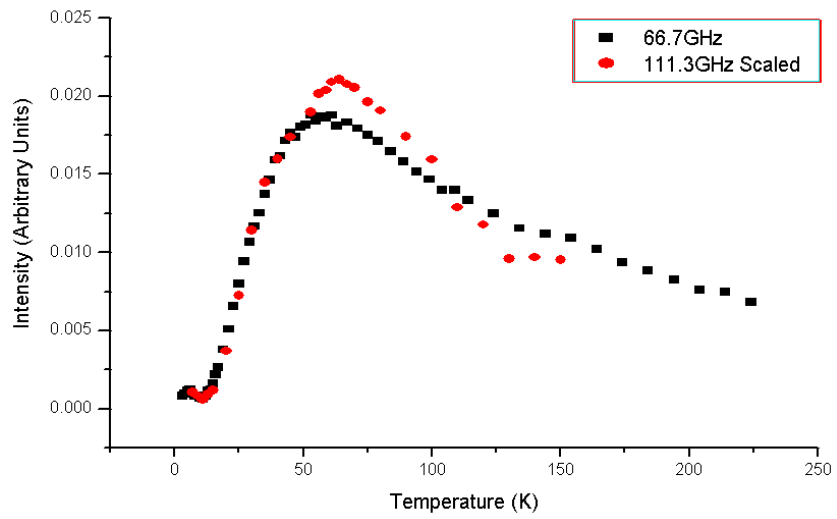


Fig. 9. Temperature dependence of signal intensity at both 66.7 GHz and 111.3 GHz.

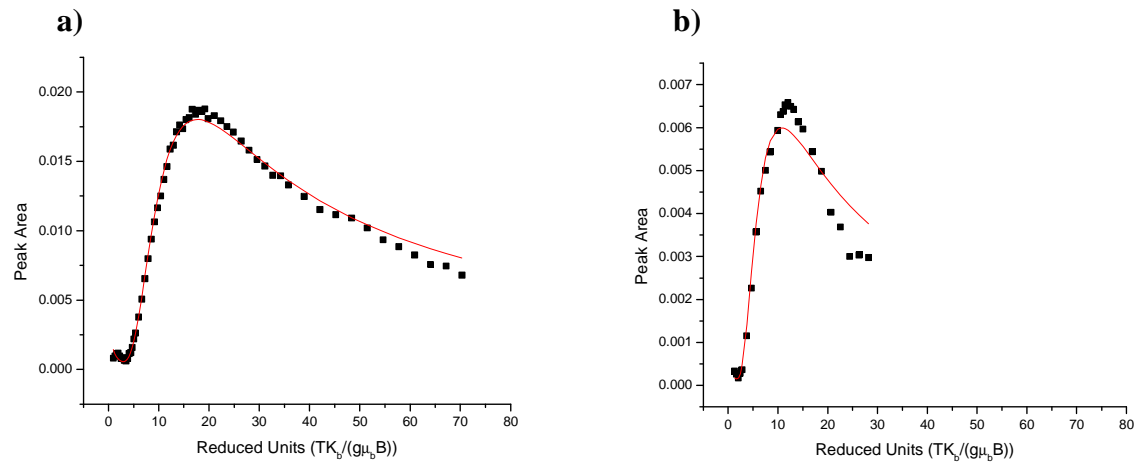


Fig. 10. a) Temperature dependence of signal intensity at 66.7 GHz fitted to Eq. (5).
 b) Temperature dependence of signal intensity at 111.3 GHz fitted to Eq. (5).